THE ASTROPHYSICAL JOURNAL, 354:220–228, 1990 May 1

DISCOVERY OF MOLECULAR HYDROGEN FLUORESCENCE IN THE DIFFUSE INTERSTELLAR MEDIUM

CHRISTOPHER MARTIN
Columbia Astrophysics Laboratory, Columbia University

AND

MARK HURWITZ AND STUART BOWYER
Space Sciences Laboratory, University of California, Berkeley
Received 1989 August 18; accepted 1989 October 9

ABSTRACT

We report the first detection of molecular hydrogen fluorescence in the diffuse interstellar medium. Using the Berkeley UVX Shuttle Spectrometer, we have observed H_2 Lyman band fluorescence in four directions, each with high significance. This is the first direct observation of the radiative byproduct of H_2 photodissociation in the diffuse interstellar medium. Molecular hydrogen fluorescence is detected in all directions that have previously been found to contain significant CO emission. We have developed a simple equilibrium model that includes attenuation of the incident UV radiation field by H_2 line and dust continuum absorption. We find that these effects must be included to obtain an accurate prediction of the emergent flux. We use this to compare the observed intensities to the observed CO and inferred H_2 column densities. We find evidence that the gas in the CO emission portions of the clouds may be clumpy, with a filling factor $f < 0.2$ and an average density $\langle n_H \rangle > 30$ cm^{-3} in most cases. There is also evidence for an extended halo of molecular gas that is not detected in CO but still produces significant H_2 fluorescence. In the case of the Ursa Major high-latitude molecular clouds, we suggest that the clumpy core and diffuse halo indicate that the cloud is currently being destroyed by the radiation field.

Subject headings: interstellar: matter — interstellar: molecules — molecular processes — radiation mechanisms

I. INTRODUCTION

Eddington (1937) first suggested that molecular hydrogen (H_2) could be an important component of the interstellar medium. It is now recognized that H_2 must play a critical role in the cooling of protostellar clouds and gas shocked in cloud collisions, H II regions, and supernovae. The first detection of H_2 in the interstellar medium was made by Carruthers (1970) using a rocket-borne ultraviolet spectrometer to observe Lyman and Werner band absorption lines. Since then, the *Copernicus* satellite has observed H_2 in absorption in the diffuse ISM along the line of sight to many OB stars (Rogerson *et al.* 1973). These observations have demonstrated that the fractional abundance of H_2 $[n(H_2)/n(H)]$ is determined primarily by the balance of formation on dust grains and destruction by photoabsorption of UV from the interstellar radiation field. In diffuse clouds the abundance is low, 10^{-6}–10^{-2}. Molecular clouds form when the cloud column density is sufficiently high that the absorption lines become self-shielding.

It was first pointed out by Duley and Williams (1980) that an observable byproduct of the destruction process is fluorescence in the Lyman and Werner bands. Absorption of a Lyman or Werner band photon leaves the molecule in an excited electronic state. If the density is not too high, radiative de-excitation follows. Ninety percent of these de-excitations are to bound states and produce a Lyman or Werner band photon. The remaining 10% deexcite radiatively to an unbound continuum level. The first detection of H_2 fluorescence in a nebula associated with a nearby star was obtained by Brown *et al.* (1981) for T Tauri and Burnham's nebula. Recently, H_2 fluorescence has been discovered from the cloud IC 63 bathed in the intense UV radiation field of a nearby B-star (Witt *et al.* 1989). In this paper we report the first detection of H_2 fluorescence in the diffuse interstellar medium and excited by the general interstellar radiation field.

II. OBSERVATIONS AND SPECTRUM RADIATION

The Berkeley Extreme Ultraviolet/Far Ultraviolet Shuttle Telescope (EUV: λλ600–1150; FUV λλ1400–1900) is a nebular spectrophotometer incorporating a fast (f/2.0) off-axis paraboloid optic with a Rowland spectrograph. The spectrometer has a field of view of 0°.1 × 4°. Imaging along the long axis of the spectrometer entrance slit is accomplished with a toroidal grating and the two-dimensional detectors allow for the identification and subsequent elimination of stellar contributions to the data. Scattering from geocoronal and airglow lines has been minimized by using filters which are placed at the detectors to eliminate the residual scattered H I λ1216 and O I λλ1304, 1356 emission. Detector internal background was measured every 90 s on orbit using a rotating shutter mechanism. Pre- and postflight calibrations were made that differed by less than 5%–10% at all $\lambda > 1300$ Å. The spectral resolution for diffuse emission was determined by calibration to be well described by a Gaussian with a FWHM of 15 Å over the full slit length. Pre and postflight wavelength calibration demonstrated wavelength accuracy of better than ± 3 Å.

The Berkeley spectrometer flew on Shuttle mission 61-C during the period of January 12–20 as part of the UVX experiment, which included an experiment built by the Johns Hopkins University (Murthy *et al.* 1989). Nine observations were performed successfully, with eight of astronomical interest.

The analysis procedure consisted of the following steps: (1) spectrum accumulation and subtraction of internal background; (2) exposure image accumulation and spectrum flat-

fielding; (3) star detection and removal. The background levels were typically 20%–30% of the total signal and showed no large secular variations. The stellar detection procedure is sensitive to stars with fluxes $F_\lambda > 10^{-14}$ ergs cm^{-2} s^{-1} Å^{-1} during pointings, and $F_\lambda \gtrsim 10^{-13}$ ergs cm^{-2} s^{-1} Å^{-1} during scans. Undetected, unresolved stars produce an average of 3 photons cm^{-2} s^{-1} sr^{-1} Å^{-1} at high galactic latitudes, or less than 2% of the observed continuum level. The instrument, observing conditions, and analysis procedures are described more fully in Martin and Bowyer (1989).

Figure 1 shows spectra obtained in the four directions for which the H_2 fluorescence appears unambiguously.[1] By far the most convincing signature of H_2 fluorescence is the presence of the strong emission in the 1570–1610 Å band. This feature is repeated consistently in the four directions and in all directions with previously measured CO emission. The only atomic feature that is known to appear in this wavelength band in astrophysical contexts is [Ne IV] λ1604, which is sometimes observed in planetary nebula spectra, but it is invariably weak relative to other high ionization lines such as C IV λ1549 and O III] λ1664. While both are detected in several of the UVX targets (Martin and Bowyer 1989), neither is present in any of the three showing the λ1605 line. We know of no other atomic line which could account for the λ1605 features.

We have fitted the spectra by assuming that they consist of two components: (1) a linearly varying continuum produced by a combination of dust scattering and two-photon continuum (Martin, Hurwitz, and Bowyer 1990), and (2) an H_2 Lyman band line and continuum spectrum as calculated by Jakobsen (1982). The H_2 spectrum is generated assuming equilibrium, optically thin conditions. We show below that modifications to these conditions do not significantly affect the spectral shape, although they do have an important influence on the interpretation of the overall intensity. We convolve the spectrum through the spectrometer Gaussian resolution kernel for comparison to the fluxed spectra. The predicted H_2 spectrum is insensitive to the interstellar radiation field spectrum

[1] Note: Murthy *et al.* 1989, use a different target numbering scheme than ours: targets 1–3 are the same, while our target 4 is the same as their target 5, our target 6 the same as their target 7, and so on for the remaining three targets. Their target 4, comet Haley is not numbered by us.

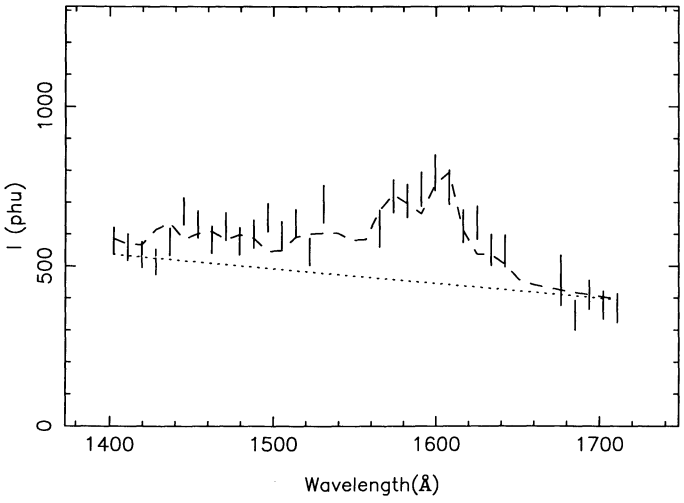

FIG. 1*a*

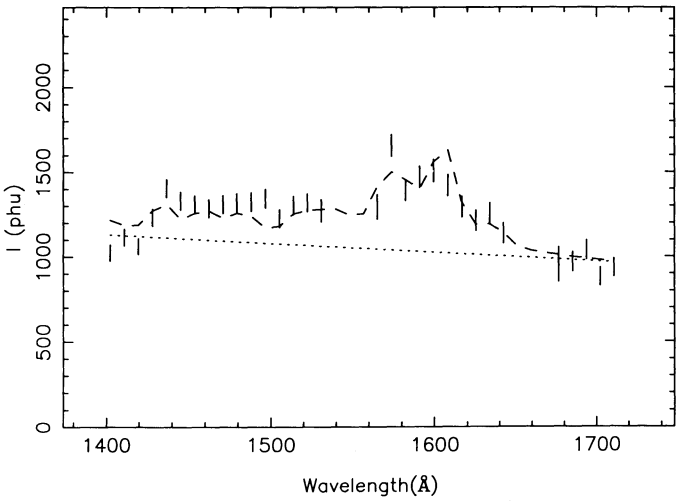

FIG. 1*b*

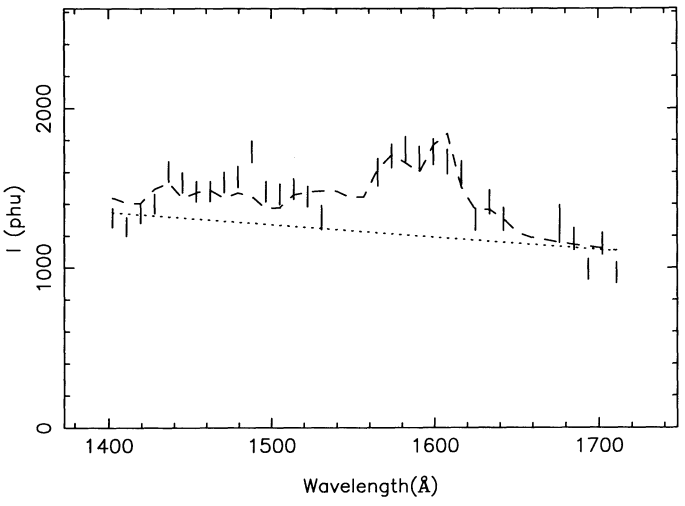

FIG. 1*c*

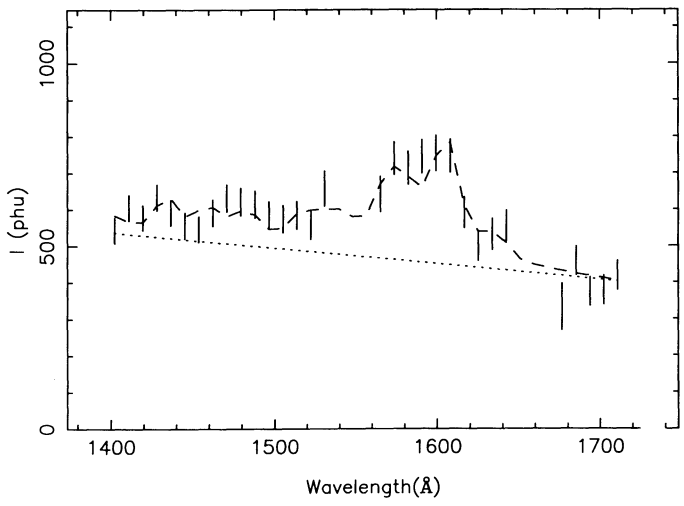

FIG. 1*d*

FIG. 1.—Fluxed, background-subtracted spectra from targets with significant H_2 fluorescence: (*a*) target 2; (*b*) target 4; (*c*) target 5; (*d*) target 6

and the degree of excitation of vibrational and rotational states in the ground electronic state. In the model fitting, the fluorescence intensity is permitted to vary, along with the slope and intercept of the linear continuum fit. We have excluded regions of the spectrum where there is a known or suspected emission feature associated with highly ionized species (Martin and Bowyer 1986). These regions are excluded even in targets that have no detectable emission, although this has virtually no effect on the results. In Figure 1, the dashed lines show the best-fit model spectra along with the flux-normalized data.

Molecular hydrogen fluorescence appears in four spectra with high significance. In each of these cases, a fit to a straight-line continuum model is very poor, giving $\chi^2 = 220$–320 for 100 degrees of freedom. Addition of the H_2 Lyman lines and continuum with only one additional free parameter (intensity), greatly improves the fits, reducing the χ^2 in each case by $\Delta\chi^2 \sim 100$–200 and resulting in a χ^2 in the range $100 < \chi^2 < 150$. Fits to a single second degree polynomial, with the same number of free parameters as the H_2 plus linear continuum model, gives chi-squares that are 50–100 higher than the H_2 fits. These results make a convincing statistical case for the presence of H_2 in these targets. This case is further strengthened by the observation that all targets containing strong CO emission (targets 4, 5, and 6) also exhibit H_2 fluorescence. We discuss this point at length below. The results of the H_2 model fits are summarized in Table 1, along with upper limits obtained from the other four targets.

We define the intensity (I_0) as the total flux in photons cm^{-2} s^{-1} sr^{-1} due to H_2 appearing in the $\lambda\lambda$1400–1700 band. Approximately 30% of the fluorescent line emission appears in the $\lambda\lambda$1400–1700 Lyman band—the remainder is emitted in the $\lambda\lambda$900–1300 Werner band. Most of the Lyman continuum band falls in the $\lambda\lambda$1400–1700 region. We also show the ratio of the fluorescence intensity to the total continuum intensity in the $\lambda\lambda$1400–1850 band.

III. FLUORESCENCE MODEL

The interpretation of the observed fluorescent intensities is quite simple if the molecular hydrogen abundance reflects the equilibrium between formation on dust grains and the destruction by photoabsorption, and if the fractional abundance $n(H_2) \ll 2n(H)$. We discuss below the conditions under which these assumptions may not hold. When they do, the total rate per unit volume of fluorescent photon production is related to the destruction rate by

$$4\pi\epsilon_0\langle k\rangle = \text{destruction rate cm}^3 .$$

The parameter $\langle k\rangle = 0.11$ is the number of absorptions that result in dissociation, calculated for a typical radiation field (to which it is not particularly sensitive). In equilibrium, the formation rate $Rn_H\, n(\text{H I})$ equals the destruction rate, and the emissivity ϵ_0 (Duley and Williams 1980; Jakobsen 1982):

$$\epsilon_{ml} = \frac{Rn_H\, n(\text{H I})}{4\pi\langle k\rangle}\, r_{ml} . \tag{1}$$

Note that $n_H = n(\text{H I}) + 2n(H_2)$. The factor r_{ml} is the probability of producing line (m, l) per absorption. The formation rate constant R has been estimated theoretically to be in the range $R = (1$–$3) \times 10^{-17}$ s^{-1} (Burke and Hollenbach 1980) depending somewhat on the grain and gas temperatures, while *Copernicus* observations also have indicated that $R = (1$–$3) \times 10^{-17}$ s^{-1} (Jura 1974). We take

$$R = 2 \times 10^{-17}\ s^{-1}$$

in the analysis below unless otherwise stated. It is important to note that the equilibrium condition renders the fluorescence intensity insensitive to the strength of the radiation field, as well as to line blocking and extinction of the incident radiation by H_2 and dust, respectively. However, the fluorescence emission is subject to extinction as it exits the cloud.

We begin with a simple model of a semi-infinite slab, where the distance into the slab is x. We assume that the total gas density n_H and the gas-to-dust ratio are constant, and that the equivalent dust cross section per H-atom is σ_d. The H_2 producing clouds are assumed to fill the field of view. Finally, dust scattering back into the field of view is ignored. The observed intensity from a slab of line of sight depth L and a run of density with depth into the cloud of $n(x)$ is then

$$I_0 = \int_0^L \frac{Rn_{H n(\text{H I})}}{4\pi\langle k\rangle} \exp\left[-\sigma_d \int_0^x n_H(\xi)d\xi\right] dx , \tag{2}$$

in (photons cm^{-2} s^{-1} sr^{-1}). This is easily solved if we assume that the density appearing in the exponential can be approximated by an average density, so that $\int_0^x n(x)dx \simeq \bar{n}x$. The observed intensity is then

$$I_0 = \frac{R\overline{n(\text{H I})}}{4\pi\langle k\rangle\sigma_d}\left(1 - e^{-\sigma_d N(\text{H})}\right) , \tag{3}$$

TABLE 1

SUMMARY OF TARGETS AND H_2 FLUORESCENCE MODEL FITS

Target Number	l	b	N(H I) (10^{20} cm^{-2})	χ^2 [a]	$\chi^2(0)$ [b]	I_0 (10^4 units) [c]	$\frac{I_0}{I_{TOT}}$ (1400–1850 Å)
1	155°	58°	1.0	...	...	<0.5	<0.10
2	132	40	3.9	130	225	3.4 ± 0.6	0.33
3	74	86	2.8	...	...	<1.0	<0.14
	237	86					
4	168	−16	11.7	128	320	5.8 ± 0.8	0.27
5	135	25	21	148	303	6.3 ± 1.0	0.25
	135	9.1					
6	142	35	3.9	98	219	3.3 ± 0.6	0.32
7	216	−39	4.5	...	...	:2.2 ± 0.8	0.18
8	335	82	2.5	...	...	<1.3	<0.16
	335	74					

[a] χ^2 obtained with linear continuum model alone.
[b] χ^2 obtained with H_2 and linear continuum.
[c] Units = photons cm^{-2} s^{-1} sr^{-1}.

where $N(H)$ is the total hydrogen column density along the line of sight. For low to moderate column density clouds, we can take $\overline{n(\text{H I})} \approx n_H$ and $N(\text{H I}) \approx N_H$. At high column densities, where a large fraction of H I is converted to H_2, the fluorescence intensity becomes quite sensitive to the details of the transition, through the factor $\overline{n(\text{H I})}(1 - e^{-\sigma_d N(H)})$. We find below, using a more exact model, that the approximation

$$\overline{N(\text{H I})} \simeq N_H\left[1 - \frac{N(H_2)}{N(H)}\right]$$

makes equation (3) accurate to within a factor of 2 at all but the highest densities. Note that the evaluation of equation (3) still requires knowledge of the total column density $N(H) = N(\text{H I}) + N(H_2)$, rather than just the H I column density. This might be obtained, for example, by 21 cm and CO observations combined.

In several of the targets, the peak H_2 column density is $N(H_2) \simeq 2 \times 10^{20}$ cm^{-2} (DeVries 1988), and therefore the H_2 absorption lines are clearly optically thick. It is therefore important to compare the approximation of equation (3) to a more exact calculation. We do that here. In general, the local emissivity in fluorescence lines is

$$\epsilon_{ml} = n(H_2)\langle(\beta_{Jm})_0 K_{Jm}\rangle_J f_{ml}\,, \qquad (4a)$$

where $(\beta_{Jm})_0$ is the upward transition rate in ground rotational state J to upper level m outside the cloud, and the attenuation factor $K_{Jm} = \int \phi(\Delta v)e^{-\tau_v}dv$ accounts for absorption in the lines. The bracket denotes an average over the rotational level occupation fractions, [e.g., $\langle F(J)\rangle_J = [\sum_J n(J)F(J)]/[\sum_J n(J)]$, which is determined by collisional and photon pumping. The factor f_{ml} is a branching ratio from upper level m to lower level l, so that $\sum_l f_{ml} = 1$. The optical depth τ_v must include the absorption by dust of radiation penetrating the cloud. The H_2 and total hydrogen densities are related (for the calculation of τ_d) again assuming equilibrium between formation and destruction (Spitzer 1978):

$$n(H_2) = \frac{Rn_H\, n(\text{H I})}{\sum_m k_m(\beta_{Jm})_0 K_{Jm}}\,.$$

The observed intensity is then

$$I_{ml} = \int \epsilon_{ml}(x)\,\exp\left[-\sigma_d(v_{ml})\int_0^x n_H(\xi)d\xi\right]dx\,. \qquad (4b)$$

For simplicity, we ignore the effects of dust scattering on the radiation field within the cloud.

We model the rotational (J-level) population using a four-level scheme similar to that of Federman, Glassgold, and Kwan (1979). This includes collisional excitation and de-excitation using rates of Shull and Hollenbach (1978), rotation-vibration cascade coefficients that model the populating effects of UV pumping (Black and Dalgarno 1976), photoabsorption and spontaneous decay via quadrupole emission. The $J = 0$ and $J = 1$ levels are assumed be maintained in thermal equilibrium at the gas temperature by H-atom and proton exchange reactions.

We have numerically integrated equation (4) over a wide range of H_2 column densities, for several values of the density. Variation of n_H has the following effect: with a larger density, the H I converts to H_2 at a lower value of the total hydrogen column $N(H)$, with correspondingly less dust attenuation as the radiation escapes the cloud. We show the calculated total H_2 fluorescent intensity in the 1400–1700 Å in Figure 2, for

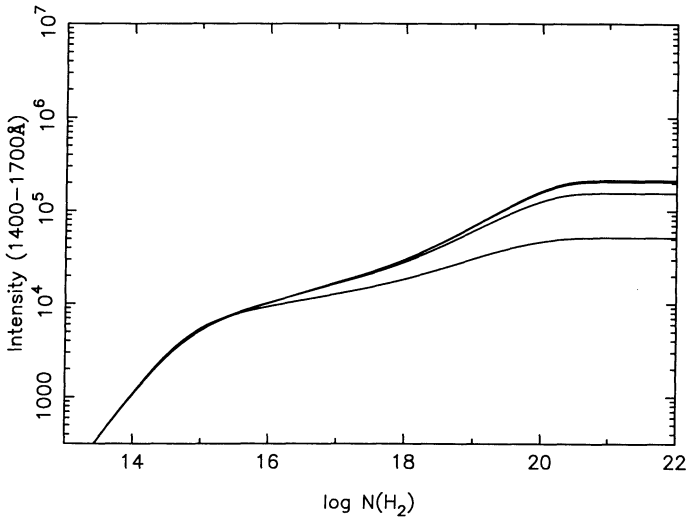

FIG. 2.—Predicted H_2 fluorescence intensity vs. $N(H_2)$, for $n_H = 10$ (*lower curves*), 100 (*middle curve*) and 10^3 (*upper curve*) cm^{-3}.

$n_H = 10{,}100$, and 10^3 cm^{-3}. For $N(H_2) < 10^{18}$ cm^{-2}, the intensity is independent of the density.

We can evaluate the accuracy of equation (3) by calculating correction factors, defined as

$$f_c = \frac{I(\text{equation [4]})}{I(\text{equation [3]})}\,.$$

This shows that equation (3) is accurate to within a factor of 2 for $N(H_2) < 10^{22}$ cm^{-2}. We use equation (4) for all subsequent analysis.

The model spectrum showing the full rotational-vibrational structure is displayed in Figure 3. The shape of the spectrum obtained at 15 Å resolution is quite insensitive to the model parameters, which principally affect the weak and unresolved higher rotational levels.

IV. ANALYSIS

a) Taurus Cloud

The Taurus region is a local ($\sim$140 pc) molecular cloud first discussed by Ungerechts and Thaddeus (1987). Target 4 was a

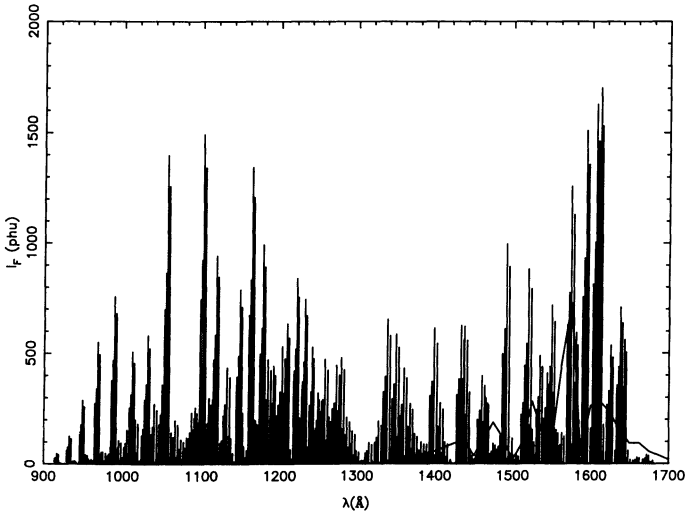

FIG. 3.—The full rotational-vibrational spectrum of H_2 fluorescence predicted by our optically thick model, for $n = 100$ cm^{-3}.

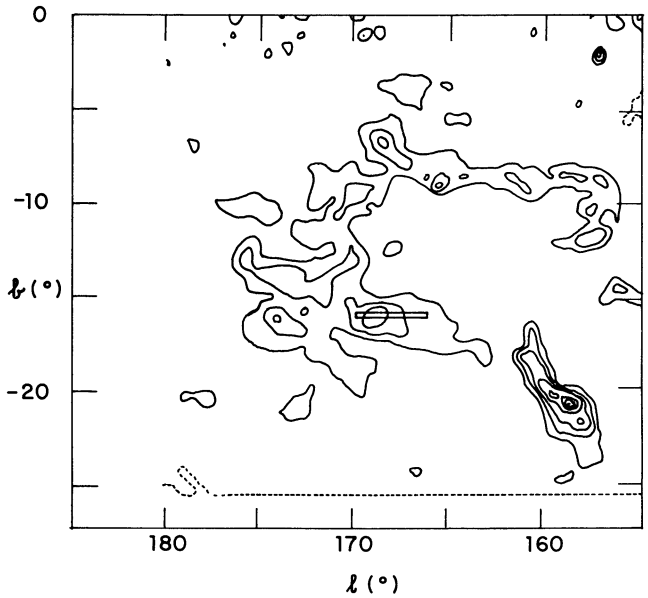

FIG. 4.—The spectrometer entrance slit for the observation of the Taurus Cloud as outlined by CO contours (DeVries 1988). Lowest contour and contour spacing is 5 K km s^{-1}.

pointed observation which included a region of this cloud, as shown in Figure 4, which was taken from Dame *et al.* (1987). We can use the observed fluorescence intensity along with the CO column density and our simple model to derive the cloud density, n_H. Dame *et al.* use a CO/H_2 conversion factor of $N(H_2)/W_{CO} = 2.7 \times 10^{20}$ cm^{-3} (K km $s^{-1})^{-1}$, implying that $N(H_2) = 3.4 \times 10^{21}$ cm^{-2} in the region of target 4. It can be seen from Figure 2 that the fluorescence intensity is sensitive to intrinsic density at this high level of $N(H_2)$. We have integrated the CO maps over the spectrometer field of view and derived the expected H_2 fluorescence intensity, allowing the cloud density to vary. We find that in order to match the observed intensity of 5.8×10^4 photons cm^{-2} s^{-1} sr^{-1}, the density must be $n_H = 16$ cm^{-3}, surprisingly low for a molecular cloud. At this low density, the total H I column density required to produce the inferred H_2 column is $N(H\ I) = 3 \times 10^{21}$ cm^{-2}. But in this direction, the total H I column density is $N(H\ I) = 10^{21}$ cm^{-2}, while that associated with only the cloud is unlikely to be greater than $\sim 4 \times 10^{20}$ cm^{-2}. With the observed H I column density, an intrinsic density of $n_H = 300$ cm^{-3} is needed to produce the observed CO. But this would produce H_2 fluorescence 5 times more intense than observed. How do we account for this discrepancy?

We used a formation rate of $R = 2 \times 10^{-17}$ cm^3 s^{-1} above. While a smaller rate is possible, a decreased R does not produce a proportional fall in the fluorescence intensity. A rate as low as 4×10^{-19} cm^3 s^{-1} would be necessary to produce consistency. We have also assumed equilibrium between formation and dissociation. However, since $N(H_2)$ and $N(H\ I)$ are known approximately, as is the radiation field, the fluorescence intensity for a homogeneous, smooth cloud is predictable directly, without relying on the equilibrium assumption.

A more likely possibility is that the H_2 is highly clumped in the cloud. Clumpiness promotes local condensations to much higher column and space densities, leading to enhanced line and dust shielding as well as increased H_2 formation rates. Evidence for clumpiness has been found in both high-latitude molecular clouds (Blitz 1986; Magnani 1987) and in larger molecular clouds (Stenholm 1986). The increase in H_2 fluorescence is not proportional to the increased column densities in the clumps, because they are optically thick in dust. Thus, clumpiness leads to a net *decrease* in the total fluorescence from the cloud of a given *average* H_2 column density.

We can estimate these effects with a simple modification to our model. If the function $I_{hom}[N(H_2), n_H]$ is the correct expression for the observed fluorescence level from a homogeneous medium, and f_V is the volume filling factor of the clumps, then the fluorescence from the clumpy medium is given by

$$I_{clump} = I_{hom}[\langle N(H_2)\rangle f_V^{-2/3}, \langle n_H\rangle f_V^{-1}] f_V^{2/3} ,$$

where $\langle N(H_2)\rangle$ is the average ("observed") H_2 column density, and $\langle n_H\rangle$ is the average total density. We have allowed the density and the filling factor to vary in order to match the observed H_2 fluorescence as well as the H_2 and H I column density constraints. Figure 5 shows the allowed region of $(\langle n_H\rangle, f_V)$ space after imposing both constraints. Note that the intrinsic density of the clumps is $\langle n_H\rangle / f_V$. It can be seen that the average density must be greater than 16 cm^{-3}, while the filling factor must be in the range $0.05 < f_V < 0.2$. With $f = 0.05$, the fluorescence intensity saturates at 60,000 photons cm^{-2} s^{-1} sr^{-1} for $\langle n_H\rangle > 100$ cm^{-3}, as the dust in the clumps becomes optically thick. We discuss below several implications of this clumpy molecular cloud structure.

A second possibility exists: if the molecular gas is surrounded by a halo of low-density gas where most of the H_2 fluorescence is formed, the high-density inner regions would be shielded by dust extinction. We have modified the H_2 fluorescence model to allow for a low-density envelope and higher density core. With $n_{env} = 10$ cm^{-3} and $n_{core} = 10^3$ cm^{-3}, the observed intensity is reproduced with a halo column density of 6×10^{20} cm^{-2}. Most of the gas is atomic, with $N(H_2) = 3 \times 10^{20}$ cm^{-2} in the halo. The halo is extended, with a thick-

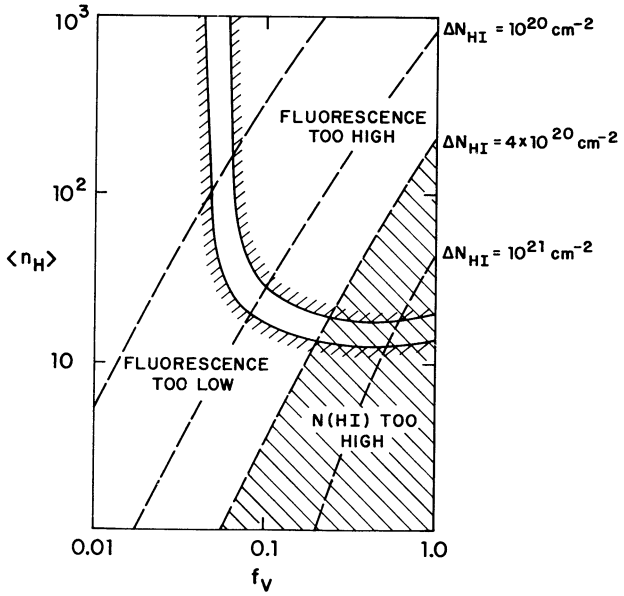

FIG. 5.—Allowed regions of parameter space of average density $\langle n_H\rangle$ and filling factor f, for target 4 in the Taurus Cloud. Parallel hatched lines bracket the required values to produce the observed H_2 fluorescence and CO emission. Dashed lines show predicted values of $N(H\ I)$ associated with the cloud. Hatched region is ruled out because too much H I is implied.

ness of 10–20 pc. As much mass is present in the halo as in higher density core. This interpretation would be consistent with evidence from high-resolution 21 cm scans of CO cloud edges for extended H I envelopes around molecular gas (Wannier *et al.* 1983). We discuss below two scanned targets which provide further evidence for this conclusion.

b) The Ursa Major Cloud

Target 6 included a scan of the Ursa Major molecular cloud complex, which is illustrated in Figure 6. The boxes show regions of the sky where the spectrometer shutter was open. Scan segments 4–6 included various portions of the cloud, with the best exposure in segment 4. The CO map was obtained by DeVries (1988). We have binned the spectra for this target into separate scan segments and used them to search for local variations in the fluorescence intensity. We have fitted each segment spectrum with the three parameter model used above. The best-fit H_2 intensities for each segment are consistent with the value obtained for the entire scan (see Table 1). Fluorescence is detected in all of the segments, with marginal evidence for a maximum in segments 3 and 4, where the CO peaks as well.

The filamentary CO core of the cloud appears to be surrounded by a halo of H_2, with insufficient column density to form detectable amounts of CO. At the same time, the core does not display a significant local increase in H_2 intensity, although a decrease may be apparent in the scan from segment 4 to segment 5. Segment 4 includes a region where an H I cloud

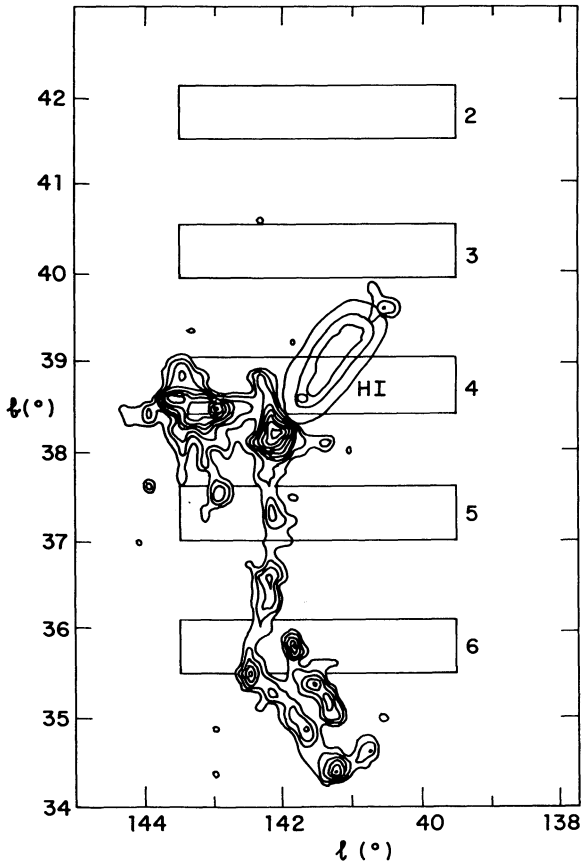

FIG. 6.—Spectrometer scan segments (shown as boxes) for the Ursa Major Cloud as outlined in CO (DeVries 1988). Lowest contour and contour spacing is 0.4 K km s^{-1}.

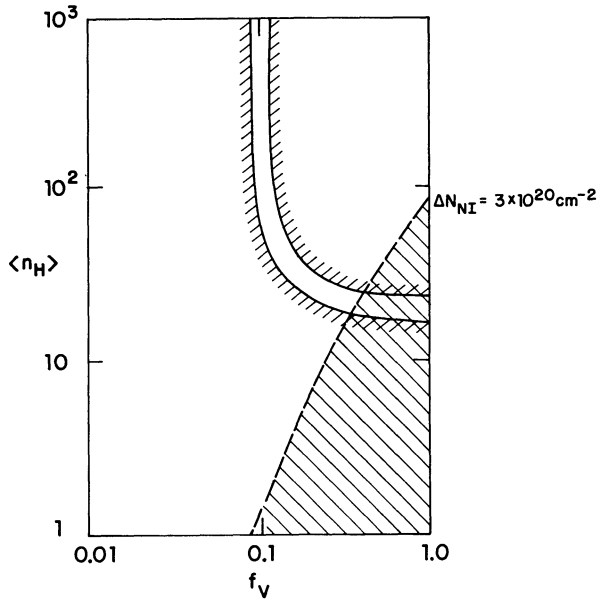

FIG. 7.—Allowed regions of parameter space of average density $\langle n_H \rangle$ and filling factor f, for target 6. Single hatched line shows upper limit to the average density (and lower limit to the filling factor) obtained by assuming that the CO core contributes no more than 15,000 photons cm^{-2} s^{-1} sr^{-1} to the H_2 fluorescence. Double hatched lines show the range of density assuming that the entire observed level is produced by the CO cloud core. Dashed lines show predicted values of N(H I) associated with the cloud. Hatched region is ruled out because too much H I is implied.

is contiguous to the CO cloud, which may indicate that one of the two are changing phase (DeVries 1988).

Assuming that the background or halo contribution to the fluorescence is relatively constant throughout the scan, with $I(H_2) \simeq 25{,}000$ photons cm^{-2} s^{-1} sr^{-1}, we can use the lack of a large enhancement in the fluorescence signal at the cloud core to place an upper limit on the density in the CO core. DeVries (1988) has derived a $N(H_2)/W_{CO}$ ratio of $0.5 \pm 0.3 \times 10^{20}$ cm^{-2} K^{-1} km^{-1} s in the Ursa Major cloud using *IRAS* 100 mm emission. (We note, however, that the lack of an fluorescence enhancement could be due to a reduction in the background fluorescence at the cloud, for example due to absorption by dust in the cloud; we discuss this point below.) In segment 4, the CO emission varies over a range of 3.6 K km s^{-1}, and therefore, the H_2 column should exhibit a peak of 1.7×10^{20} cm^{-2}. With $n_H = 30$ cm^{-3} and unity filling factor in the cloud, the fluorescence intensity would increase by 15,000 photons cm^{-2} s^{-1} sr^{-1} moving from segments 3 to 4. However, this would require a larger H I column density than is observed to form the CO column density in this region. Allowing for clumping as we did in the previous target, the limits on the allowed density and filling factor of the cloud core are given in Figure 7. The filling factor in the core must be less than 0.2.

The background fluorescence intensity, $I(H_2) \simeq 25{,}000$ photons cm^{-2} s^{-1} sr^{-1}, may or may not be directly associated with the cloud. The Ursa Major cloud complex is at a high galactic latitude and is likely to be local. The covering factor for high-latitude molecular clouds is small (Blitz 1986; DeVries 1988; Desert, Bazell, and Boulanger 1988), less than a few percent. It is unlikely that a second molecular cloud is superposed by chance. We believe it is probable that the background H_2 fluorescence is produced by an extensive molecular "halo"

surrounding the CO emission core. In the halo, the CO limits imply that $N(H_2) < 2 \times 10^{19}$. This limit, the known H I column density, and the fluorescence intensity are consistent with $n_H = 30$ cm^{-3} and $f = 1$. This would produce $N(H_2) = 1.8 \times 10^{18}$ cm^{-2}, a factor of 10 below the sensitivity of the DeVries map. Smaller average densities and filling factors are possible, with $\langle n_H \rangle / f \sim 30$ cm^{-3}, but the lack of detectable CO places a lower limit on the filling factor of $f > 0.15$. These conclusions suggest that the cloud may consist of a clumpy core surrounded by a more uniform molecular halo.

d) Target 5

Target 5 was a long scan over a large range of H I column density, at moderately low galactic latitudes ($b = 21°$–$9°$). This target has the highest H_2 fluorescence intensity. The scan includes several regions of molecular gas detected in the survey of Dame *et al.* (1987), illustrated in Figure 8. These clouds, part of the Lindblad complex, are likely to be local, given their velocity and comparatively high galactic latitudes. We have examined the segment-by-segment data to search for an enhancement in H_2 fluorescence that might be expected in moving from segments 2 to 4. Fluorescence was detected with 2.5–4 s significance in segments 1–5, with intensities consistent with the value obtained for the entire scan. As in the case of target 6, the detection of significant H_2 outside of regions of strong CO indicates a substantial background of molecular gas that does not form detectable CO. Again there are two possible explanations. The lack of a strong enhancement in the H_2 fluorescence in passing from segment 2 to segments 3 and 4 could be indicative of clumpy molecular gas in the CO clouds. The increase is less than 25,000 photons cm^{-2} s^{-1} sr^{-1}, which rules out the upper right hand region of the $\langle n_H \rangle - f$ diagram of Figure 9. While the total H I column density in the region of segment 4 is high [N(H I)] $= 3 \times 10^{21}$ cm^{-2}, examination of the relationship of the H I contours to the CO cloud distribution suggests that only $\sim 4 \times 10^{20}$ cm^{-2} of H I is associated with the CO cloud in question. This leads to a second constraint on the density and filling factor, also shown in Figure 9. This would imply a filling factor of $f < 0.3$ in the CO cloud.

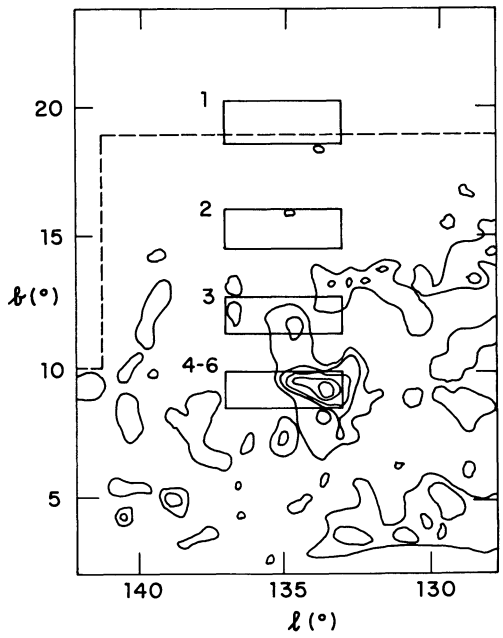

FIG. 8.—Spectrometer scan segments (shown as boxes) for the target 5 region with CO contours from Dame *et al.* (1988). Lowest contour and contour spacing are 5 K km s^{-1}.

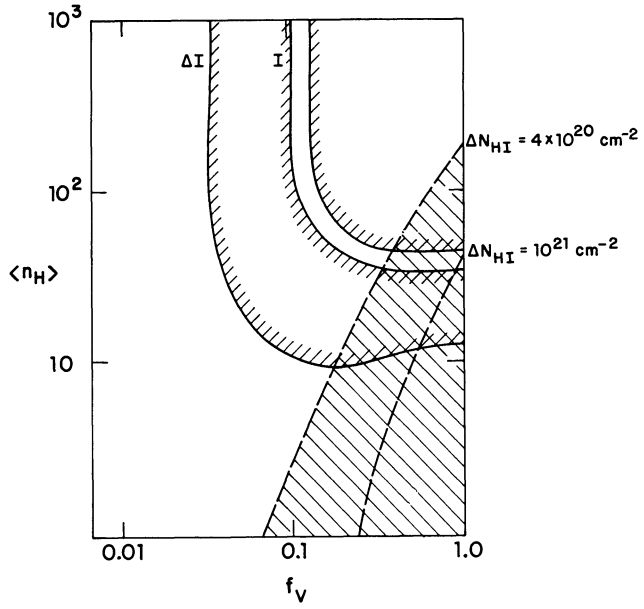

FIG. 9.—Allowed regions of parameter space of average density $\langle n_H \rangle$ and filling factor f, for target 5. Hatched parallel lines show the required values to produce the observed H_2 fluorescence and CO emission. Dashed lines show predicted values of N(H I) associated with the cloud. Hatch region is ruled out because too much H I is implied.

The lack of a peak could also be due to a low-density halo of H I/H_2 gas surrounding the CO-emitting molecular core. This would explain both the relatively low H_2 intensities as compared to those that would be predicted for CO-bearing gas, and the presence of emission in the regions surrounding the CO clouds. The envelope properties would be quite similar to those derived for the Taurus cloud in § IV*a*.

e) H_2 Fluorescence in Directions with No Known Molecular Gas

Molecular hydrogen fluorescence appears in all of the observed targets with previously detected molecular gas. Target 2 is not known to contain CO and does not coincide with a far-IR excess (Desert *et al.* 1988). However, it too displays significant H_2 fluorescence. Since we do not know the CO or H_2 column densities, we must analyze this field using H I and dust column densities. The H I column density is N(H I) $= 4 \times 10^{20}$ cm^{-2}, while the *IRAS* 100 mm data show no evidence for an enhancement in the dust column density over that expected for this H I level (Desert *et al.* 1988). For each possible value of average density $\langle n_H \rangle$ and filling factor f, we have derived the *maximum* possible H_2 fluorescence intensity consistent with those column density limits. We show in Figure 10 the density lower limit as a function of the filling factor. The average density must be greater than 10 cm^{-3}, while the intrinsic density must be less than 30 cm^{-3}. An H_2 column density in the range of $10^{19} < N(H_2) < 10^{20}$ cm^{-2} must be present, with the lowest column applying to the largest filling factor.

This implies that a significant fraction (25%–50%) of the hydrogen along this high-latitude line of sight is located in diffuse clouds with $n_H > 30$ cm^{-3}, rather than in the intercloud

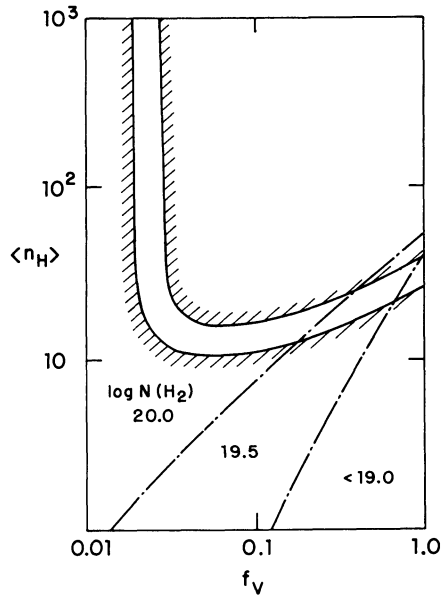

FIG. 10.—Allowed regions of parameter space of average density $\langle n_H \rangle$ and filling factor f, for target 2. Solid lines show the required values to produce the observed H_2 fluorescence while not overproducing N(H). Dot-dashed lines are contours of predicted $N(H_2)$.

medium. This conclusion is also consistent with our detection of substantial H_2 outside of the CO clouds in the Ursa Major region and in target 5.

f) Regions with No H_2 Fluorescence

The upper llmits to H_2 fluorescence in three directions (targets 1, 3, and 8) can be used to constrain the density and filling factor of gas along these sightlines. In each of the targets, the intrinsic density $n_H = \langle n_H \rangle / f < 15$ cm^{-2}. The H_2 column density in these directions is still a sensitive function of the intrinsic density and filling factor. For example, in target 1, $N(H_2) < 10^{16}$ cm^{-2} for $f = 1$, but $N(H_2) < 17.5$ cm^{-2} for $f = 0.1$. Even so, the fraction of mass present in molecular form is apparently less than 1% in these directions.

IV. DISCUSSION

Our detection of H_2 fluorescence represents the first time that this process has been observed in the diffuse interstellar medium. Fluorescence is detected with high significance in every target that also contains CO emission. The agreement of the observed fluorescence intensities with the predictions of simple equilibrium theory provides strong and direct confirmation of the model of H_2 formation on dust grains and destruction by UV photoabsorption.

We have developed a simple model to predict the H_2 fluorescence intensity in clouds that are optically thick in dust and H_2 lines. We find that dust absorption produces a sensitive interdependence between the H_2 fluorescence intensity, the H_2 column density, the intrinsic density and the filling factor of the molecular gas.

We have found that in several cases, clumpy molecular gas may be indicated in order to both form sufficient CO and not overproduce the H_2 fluorescence. Clumpiness has been suggested to explain the CO observations alone for small and large molecular clouds. For example, Blitz (1986) estimates the filling factor to be $f_V \sim 0.1$ in high-latitude molecular clouds, with intrinsic densities of $n_H \sim 3000$ cm^{-3}. These parameters are consistent with those we derive. These clumps may be related to the formation of low-mass stars or even substellar objects (Blitz 1986).

Alternatively, the observation of low fluorescence intensity and emission in the regions around CO clouds may be evidence for low-density halos surrounding molecular clouds. These halos would be extended, largely H I, and contain as much mass as the molecular interior. While 5%–30% of the halo gas would be in H_2, the low densities and large UV photodissociation rates would prevent the formation of detectable amounts of CO.

In directions without H_2 fluorescence, our measurement of the average density is in accord with 21 cm observations which indicate that a significant fraction of the H I gas is in lower density phase than the canonical diffuse cloud with $n = 40$ cm^{-3}. Also, since the ratio of fluorescence to continuum intensity (which reflects the relative contributions of H_2 to dust scattering) is less than 0.3 over the $\lambda\lambda$1400–1850 band, previous estimates of the contribution of dust scattering to the ultraviolet background that did not account for H_2 have not been significantly in error.

Our analysis is based on the assumption that the H_2 is in equilibrium. For the H_2 abundance to be in equilibrium, the typical diffuse cloud must be older than a formation time scale $\tau(H_2) = [Rn]^{-1} = 4 \times 10^7 (40 \text{ cm}^{-3}/n)(2 \times 10^{17} \text{ s}^{-1}/R)$ yr. Equilibrium may pertain to the cloud clumps, but is less likely to hold in the diffuse halos. Many processes occurring in the interstellar medium can change the density and phase of a gas element, including cloud-cloud collisions due to random motions and spiral shocks, evaporation in a hot substrate, and condensation in radiative cooling supernova shells.

The proximity of an H_2 region in the Ursa Major cloud is circumstantial evidence for a phase change in one of our targets (DeVries 1988). Because the formation time scale of the H_2 in the halo is 5×10^7 yr, it is unlikely that the H_2 in the halo is formed at that low density. The H_2 is more easily and rapidly formed in a high-density regime, such as a radiative supernova or stellar wind shock. We propose therefore that the diffuse cloud halo is a byproduct of the photodissociation of dense molecular clumps by the UV radiation field. The clumpy inner core is best protected against the radiation field and therefore is the last portion of the cloud to be destroyed.

Future observations of H_2 fluorescence with higher sensitivity, spectral, and spatial resolution will be critical for an intercomparison with high-resolution CO, infrared, extinction, and H I maps. By carefully associating the atomic and molecular gas, and dust, and by resolving density sensitive rotational transitions in the fluorescence spectrum, it will be possible to make a detailed exploration of the physical conditions, morphology, and ultimately the origin and fate of small molecular clouds.

We are grateful to Charles Pellerin of NASA Headquarters, who made possible the use of Get Away Specials for forefront astrophysical research. This work has been supported by NASA grants NAG 5-642 and NGR 05003450.

REFERENCES

Black, J. H., and Dalgarno, A. 1976, *Ap. J.*, **203**, 132.
Blitz, L. 1986, in *Proc. NATO Advanced Science Institute, Physical Processes in Interstellar Clouds*, ed. G. E. Morfill and M. Scholer (Dordrecht: Reidel), p. 35.
Brown, A., Jordan, C., Millar, T. J., Gondhalekar, P., and Wilson, R. 1981, *Nature*, **290**, 34.
Burke, J. R., and Hollenbach, D. J. 1980, NASA Tech. Memo 81163.
Carruthers, G. 1970, *Ap. J.* (*Letters*), **161**, L81.
Dame, T. M., *et al.* 1987, *Ap. J.*, **322**, 706.
Desert, F. X., Bazell, D., and Boulanger, F. 1988, *Ap. J.*, **334**, 815.
DeVries, H. W. 1988, Ph.D. thesis, Columbia University.
Duley, W. W., and Williams, D. A. 1980, *Ap. J.* (*Letters*), **242**, L179.
Eddington, A. S. 1937, *Observatory*, **60**, 99.
Federman, S. R., Glassgold, A. E., and Kwan, J. 1979, *Ap. J.*, **227**, 466.
Jakobsen, P. 1982, *Astr. Ap.*, **106**, 375.
Jura, M. 1974, *Ap. J.*, **191**, 375.
Magnini, L. G. 1987, Ph.D. thesis, University of Maryland.
Martin, C., and Bowyer, S. 1990, *Ap. J.*, **338**, 677.
Martin, C., Hurwitz, M., Bowyer, S. 1990, in preparation.
Murthy, J., Henry, R. C., Feldman, P. D., Tennyson, P. D. 1989, *Ap. J.*, **336**, 954.
Rogerson, J. B., Spitzer, L., Drake, J. F., Dressler, K., Jenkins, E. B., Morton, D. C., York, D. G. 1973, *Ap. J.* (*Letters*), **181**, L97.
Shull, J. M., and Hollenbach, D. J. 1978, *Ap. J.*, **219**, 877.
Spitzer, L. 1978, *Physical Processers in the Interstellar Medium* (New York: Wiley).
Stenholm, L. G. 1986, in *Proc. NATO ASI Physical Processes in Interstellar Clouds.*
Ungerechts, H., and Thaddeus, P. 1987, *Ap. J. Suppl.*, **63**, 645.
Wannier, P. G., Lichten, S. M., Morris, M. 1983, *Ap. J.*, **268**, 727.
Witt, A. N., Stecher, T. P., Boroson, T. A., and Bohlin, R. C. 1989, *Ap. J.* (*Letters*), **336**, L21.

STUART BOWYER and MARK HURWITZ: Space Sciences Laboratory, University of California, Berkeley, CA 94720

CHRISTOPHER MARTIN: Columbia Astrophysics Laboratory, Columbia University, New York, NY 10027